SUSTAINABLE ENGINEERING

(eISSN:3083-8231)
*Article*
**Volume 3, 2026**
https://doi.org/10.51200/susten.v3i1.7699

# Prediction of Methylene Blue and Congo Red Removal in *Lemna minor* Phytoremediation Using Neural-Wiener Modelling

**Sudibyo Sudibyo[1], Anton Sapto Handoko[1], Iin Nur Aini[2], Rifky Fauzi[2], Dear Michiko Mutiara Noor[2], Tiara Shofi Edriani[2], Ashraf Azmi[3], Fakhrony Sholahudin Rohman[4*], and Yudha Gusti Wibowo[5]**

[1] Research Center for Mining Technology, National Research and Innovation Agency (BRIN), South Lampung-35352, Indonesia
[2] Department of Mathematics, Institute Technology of Sumatera, Bandar Lampung, Indonesia
[3] Faculty of Chemical Engineering, Universiti Teknologi MARA Shah Alam, 40450 Shah Alam, Selangor, Malaysia.
[4] Faculty of Engineering, Universiti Malaysia Sabah, 88400, Kota Kinabalu, Malaysia,
[5] Sustainable Mining and Environmental Research Group, Department of Mining Engineering, Institut Teknologi Sumatera, Lampung 35365, Indonesia.
*Correspondence: fakhrony@ums.edu.my

*ORCID ID: 0009-0001-0220-9145
**Received: 26 May 2026, Accepted: 17 September 2026**

**Abstract:** Methylene blue and Congo red are synthetic dyes commonly found in industrial wastewater. These dyes can affect water quality and pose risks to human health and the environment. Phytoremediation using *Lemna minor* offers a simple and environmentally friendly method for reducing dye concentrations in wastewater. However, the phytoremediation process usually requires a long treatment time. Therefore, this study applied neural network-based model, namely Neural–Wiener model, to predict the percentage removal of methylene blue and Congo red during phytoremediation using *Lemna minor*. The model was trained using different data-splitting ratios for training, validation, and testing, as well as different numbers of hidden nodes. The results showed that the Neural–Wiener model provided a good prediction performance. The optimum model was obtained using 35% training data, 30% validation data, and 35% testing data with 140 hidden nodes. The optimum model achieved MSE, MAE, and WMAPE values of $5 \times 10^{-4}$, $1 \times 10^{-4}$, and $1 \times 10^{-5}$, respectively, based on the percentage removal response used as the model output. These results indicate that the Neural–Wiener model is more suitable than other models for predicting the removal performance of methylene blue and Congo red in the *Lemna minor* phytoremediation process.

**Keywords:** phytoremediation; Neural–Wiener model; neural network; methylene blue; Congo red.
© 2026 by UMS Press.

## 1. Introduction

Industrial wastewater containing synthetic dyes remains an important environmental concern because many dyes are chemically stable, highly visible even at low concentrations, and resistant to natural degradation. Methylene blue and Congo red are widely used in textile, colouring, printing, and related industrial activities. Their release into water bodies can reduce light penetration, disturb aquatic ecosystems, and adversely affect water quality. The different ionic and chemical characteristics of these dyes also make their simultaneous treatment

challenging, particularly when a treatment process must respond to changes in concentration over time [1].

Phytoremediation using aquatic plants offers a comparatively simple and environmentally compatible method for reducing contaminants in wastewater. Among the available hydrophytic plants, *Lemna minor* has attracted attention because of its rapid growth, extensive contact with the water surface, and ability to tolerate a range of wastewater conditions. The plant may contribute to contaminant removal through adsorption onto plant surfaces, uptake into plant tissues, and interactions with microorganisms associated with the root system. However, the performance of *Lemna minor* phytoremediation is not constant and may vary with dye concentration, exposure time, plant condition, and wastewater characteristics [2].

A major practical limitation of phytoremediation is that its treatment response develops gradually and may exhibit complex time-dependent behaviour. Experimental assessment commonly relies on concentration measurements taken at selected treatment times. Although these measurements provide useful information about removal performance, they do not fully describe the dynamic relationship between the initial conditions and the subsequent treatment response. Conducting additional experiments for every possible operating condition would also require considerable time and resources. Therefore, a predictive modelling approach is needed to represent the process behaviour and estimate treatment performance under different conditions [3]. The models were developed to predict the removal percentages of methylene blue and Congo red during phytoremediation using *Lemna minor*.

Conventional linear models may not adequately describe the nonlinear and time-dependent behaviour of dye removal. Although static artificial neural networks can represent nonlinear input–output relationships, they do not explicitly account for process dynamics. Block-oriented nonlinear models combine linear dynamics with static nonlinear transformations. In the Hammerstein structure, a nonlinear block precedes the linear dynamic block; in the Wiener structure, it follows the dynamic block; and in the Hammerstein–Wiener structure, nonlinear blocks are placed on both sides of the dynamic block. These structures offer different ways to represent process memory and nonlinear treatment responses [4, 5].

Several studies have demonstrated the applicability of these structures to water and wastewater systems. Frącz applied a Hammerstein–Wiener structure to an activated-sludge process to describe nonlinear relationships involving nitrogen transformations and aeration-related process behaviour. This application showed that the block-oriented structure could represent complex biological wastewater-treatment dynamics that are difficult to describe using a simple linear model [6].

Gaya et al. compared a Hammerstein–Wiener model with an artificial neural network for estimating turbidity in a water-treatment plant using experimental operating data. Although the neural network provided better accuracy in that particular case, the study demonstrated that both approaches could serve as data-driven alternatives when conventional mathematical models could not adequately represent turbidity behaviour. The findings also indicate that model structure should be evaluated objectively rather than assuming that a more complex model will always provide better predictions [7].

Abba et al. subsequently compared a general regression neural network, Hammerstein–Wiener model, nonlinear autoregressive model with exogenous inputs, and least-squares support vector machine for multiparametric modelling of a water-treatment plant. The Hammerstein–Wiener model showed strong simulation capability for hardness, turbidity, and suspended solids, whereas the relative performance differed among the measured water-quality parameters. This illustrates the benefit of block-oriented models for simultaneously analysing several treatment responses and confirms the importance of comparing alternative model structures for each application [8].

More recently, Hammerstein–Wiener modelling has been combined with supervised machine learning to predict salinity behaviour in treated wastewater. The model was selected because its structure can capture both linear dynamics and nonlinear relationships among water-quality variables. Such applications demonstrate that these models can provide useful predictive information for treatment assessment, water-quality monitoring, and operational decision-making [9].

Neural Wiener models also offer advantages for model-based prediction and control. Ławryńczuk developed nonlinear predictive-control algorithms based on neural Wiener models in which the model or predicted trajectory was linearised online to reduce the computational burden of nonlinear optimisation. This demonstrates that an accurately identified neural Wiener model can potentially be extended beyond offline simulation to process optimisation and predictive control. Han and Qiao also demonstrated nonlinear model predictive control in a wastewater-treatment application, supporting the potential of such models for predicting and regulating biological treatment systems [10, 11].

The principal benefits of applying these block-oriented neural models are therefore their ability to capture process dynamics, represent nonlinear treatment behaviour, and provide predictions without requiring a complete mechanistic description of every biological and physicochemical interaction. They may also be used as soft sensors when continuous laboratory measurements are unavailable and may provide a modelling basis for future process monitoring, optimisation, and control [5, 11].

Despite these developments, previous studies have primarily considered activated-sludge treatment, conventional water-treatment plants, turbidity, salinity, and industrial process systems. The use of Neural Wiener model for the simultaneous prediction of methylene blue and Congo red removal during *Lemna minor* phytoremediation remains underexplored. The present study addresses this gap by evaluating the three structures under consistent data-partitioning and hidden-node conditions using prediction error and computational-time criteria. Accordingly, the problem addressed in this study is the absence of a sufficiently evaluated dynamic nonlinear model for predicting the treatment response of *Lemna minor* phytoremediation involving two chemically different dyes. Without an appropriate predictive model, the interpretation of process behaviour remains dependent on individual experimental observations, and the selection of a suitable model structure becomes uncertain.

This study therefore develops and evaluates Neural Wiener model for predicting methylene blue and Congo red removal during phytoremediation using *Lemna minor*. The models are assessed under different training, validation, and testing ratios and different numbers of hidden nodes. Their performance is compared using mean squared error, mean absolute error, weighted mean absolute percentage error, and computation time. The main contribution of this work is an evaluation of block-oriented neural-network structure for representing the dynamic and nonlinear behaviour of a dual-dye phytoremediation system. The findings provide a modelling basis for predicting treatment performance and supporting future process analysis and optimisation.

## 2. Materials and Methods

### *2.1. Materials*

*Lemna minor*, known as duckweed, is a small free-floating aquatic plant from the family Lemnaceae, as shown in Figure 1(a) [12, 13]. *Lemna minor* is commonly used in phytoremediation due to its ability to control pollutants in wastewater [13, 14].



(a) (b) (c)

**Figure 1.** (a) *Lemna Minor* plant; (b) Methylene blue; (c) Congo red

Methylene blue, shown in Figure 1(b), is a cationic dye widely used in textile dyeing, paper colouring, ink production, and cosmetics [15, 16]. According to the Decree of the Minister of Environment Kep-51/MENLH/10/1995 on liquid waste quality standards, the allowable concentration range for methylene blue in wastewater is 5–10 mg/L [17]. Congo red, shown in Figure 1(c), is a synthetic dye commonly used in biochemistry and analytical chemistry for the identification and evaluation of certain compounds [18].

### *2.2 Experimental Work and Dataset Preparation*

The experimental data were obtained from phytoremediation tests conducted at the Tanjung Bintang Mining Technology Research Center and the Mining Engineering Laboratory of Institut Teknologi Sumatera. Synthetic wastewater containing methylene blue and Congo red at initial concentrations of 20, 40, 60, 80, and 100 ppm was treated with 2 g of fresh *Lemna minor* in 200 mL glass containers with a diameter of 9 cm. Water volume, container diameter, and plant mass were kept constant throughout the experiments.

The raw data in Table 1 were processed into the model input and output datasets shown in Tables 2 and 3. Table 1 presents the experimental conditions, including the initial concentrations of methylene blue and Congo red in ppm, water volume, container diameter, and *Lemna minor* mass. Since water volume, container diameter, and plant mass were kept constant at 200 mL, 9 cm, and 2 g, respectively, these variables were treated as controlled variables. The main varying data were the methylene blue and Congo red concentration profiles across the 25 experimental observations.

**Table 1**. Experimental conditions and observation indices for the *Lemna minor* phytoremediation dataset

| Observation index | Methylene blue Initial Concentration (ppm) | Congo red Initial Concentration (ppm) | Water Volume (ml) | Glass Diameter (cm) | Mass of *Lemna Minor* Plant (g) |
|---|---|---|---|---|---|
| 1 | 20 | 20 | 200 | 9 | 2 |
| 2 | 40 | 40 | 200 | 9 | 2 |
| 3 | 60 | 60 | 200 | 9 | 2 |
| 4 | 80 | 80 | 200 | 9 | 2 |
| 5 | 100 | 100 | 200 | 9 | 2 |
| 6 | 20 | 20 | 200 | 9 | 2 |
| 7 | 40 | 40 | 200 | 9 | 2 |
| 8 | 60 | 60 | 200 | 9 | 2 |
| 9 | 80 | 80 | 200 | 9 | 2 |
| 10 | 100 | 100 | 200 | 9 | 2 |
| 11 | 20 | 20 | 200 | 9 | 2 |
| 12 | 40 | 40 | 200 | 9 | 2 |
| 13 | 60 | 60 | 200 | 9 | 2 |
| 14 | 80 | 80 | 200 | 9 | 2 |
| 15 | 100 | 100 | 200 | 9 | 2 |
| 16 | 20 | 20 | 200 | 9 | 2 |
| 17 | 40 | 40 | 200 | 9 | 2 |
| 18 | 60 | 60 | 200 | 9 | 2 |
| 19 | 80 | 80 | 200 | 9 | 2 |
| 20 | 100 | 100 | 200 | 9 | 2 |
| 21 | 20 | 20 | 200 | 9 | 2 |
| 22 | 40 | 40 | 200 | 9 | 2 |
| 23 | 60 | 60 | 200 | 9 | 2 |
| 24 | 80 | 80 | 200 | 9 | 2 |
| 25 | 100 | 100 | 200 | 9 | 2 |

For model input preparation, the measured dye concentrations were converted into percentage concentration profiles relative to the reference concentration level. The value of 100% represents the reference concentration, while the following values represent the remaining dye concentration during treatment. This conversion was applied to both methylene blue and Congo red to place the input variables on a common percentage basis. The processed concentration profiles were then used as the input variables in Table 2.

The model output dataset in Table 3 was prepared using the corresponding dye removal responses. The removal response represents the percentage reduction of methylene blue and Congo red during phytoremediation. These processed input and output datasets were then used to train, validate, and test the Neural–Wiener model. This processing step ensured that the model used consistent percentage-based variables rather than directly combining raw ppm values with removal responses.

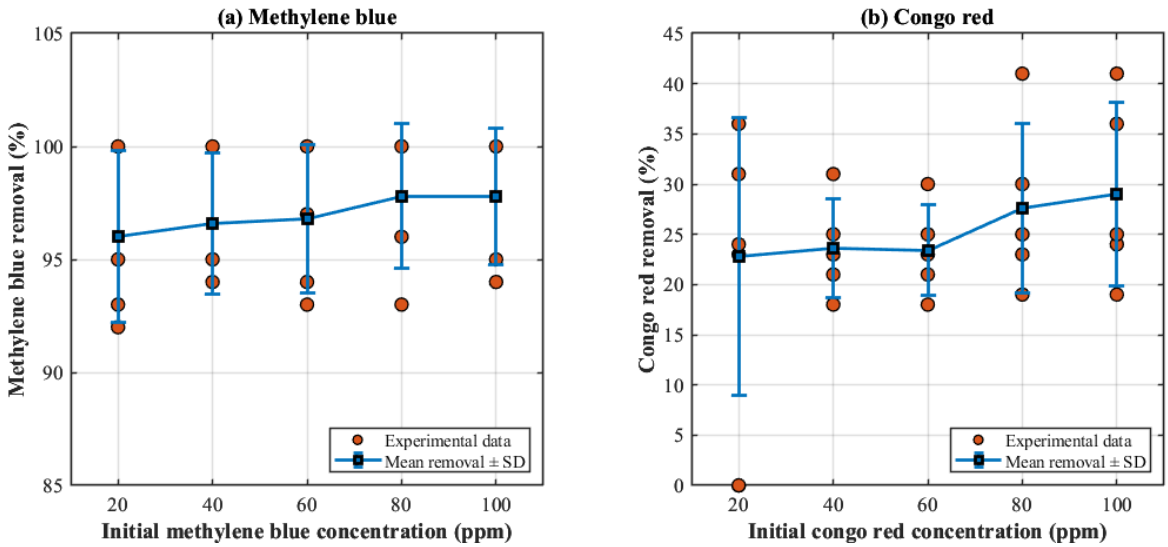



**Figure 2.** Relationship between initial dye concentration and observation-level removal response for methylene blue and Congo red. Each point represents one experimental observation from the 25-observation dataset, not a continuous daily time-series measurement.

Figure 2 shows the relationship between the initial dye concentration and the observed removal percentages of methylene blue and Congo red. The repeated observations show considerable variability, particularly for Congo red, while the mean responses change relatively gradually across the investigated concentration range. Therefore, this plot is used primarily to describe the experimental variability and overall concentration–response trend, rather than to establish nonlinearity. The initial concentrations were tested at repeated levels of 20, 40, 60, 80, and 100 ppm, and each point represents one observation from the 25-observation dataset. The figure should therefore be interpreted as an observation-level concentration–response plot rather than as a continuous time-series profile. The experimental results show noticeable variation among repeated observations at each concentration level, particularly for Congo red. However, this scatter should not be considered direct evidence of a nonlinear relationship between initial dye concentration and removal efficiency. The mean removal values change relatively gradually over the investigated concentration range. Methylene blue removal remains consistently high and increases slightly with increasing initial concentration, whereas Congo red shows a similar overall trend but with considerably greater variability among repeated observations.

The wider dispersion observed for Congo red indicates that its removal by *Lemna minor* was less consistent under the tested conditions. This variation may be associated with experimental variability, biological response, or differences in dye–plant interactions. However, because the dataset contains only 25 observations, the underlying cause cannot be determined conclusively, and the concentration–response trends should therefore be regarded as exploratory.

These results also indicate that the relationship between initial concentration and mean removal is not strongly nonlinear within the tested range. Accordingly, the use of the Neural–Wiener model in this study is not justified solely by the shape of the initial concentration–removal relationship. Rather, the model was selected to represent the overall input–output behaviour of the processed concentration profiles and removal responses. The linear state-space component accounts for the sequential and dynamic behaviour of the dataset, while the neural-network

block provides flexibility to represent possible departures from a purely linear dynamic relationship. This interpretation avoids attributing experimental scatter directly to nonlinearity and provides a more appropriate justification for the Neural–Wiener modelling approach.

Tables 1–3 present three different representations of the same 25-observation dataset. Table 1 lists the experimental conditions associated with each Observation Index, including the nominal initial concentrations of methylene blue and Congo red. The Observation Index serves only as a data identifier and does not represent a sequential treatment day. Table 2 presents the processed concentration variables used as model inputs, while Table 3 presents the corresponding removal responses used as model outputs. Therefore, the values in Table 2 should not be interpreted as direct percentage conversions of the nominal initial concentrations reported in Table 1. Instead, they represent processed concentration-profile variables obtained during data preparation. The same Observation Index is maintained across all three tables to preserve the correspondence between experimental conditions, processed inputs, and model outputs.

It should be noted that the entries from Day 1 to Day 25 do not represent a sequential daily replacement experiment in which the final concentration from one day became the initial concentration for the following day. Instead, the term “Day” is used as the observation or data index for the experimental dataset. The initial dye concentrations were arranged in repeated levels of 20, 40, 60, 80, and 100 ppm, while the water volume, glass diameter, and *Lemna minor* mass were kept constant at 200 mL, 9 cm, and 2 g, respectively. Therefore, the next observation does not depend on the previous observation’s final concentration.

The experimental data will then be processed and produce the following data. The processed input data in Table 2 were obtained by converting the measured dye concentration changes into percentage concentration profiles relative to the experimental concentration basis. The value of 100% on Day 1 represents the reference concentration level used for the processed profile. The subsequent values describe the remaining concentration trend during the treatment period. The same processing approach was applied to both methylene blue and Congo red so that the two dye-removal responses could be compared using a common percentage basis.

Table 2 presents the processed dye concentration profiles used as model input data. The values are expressed as percentage remaining concentration, not raw final concentrations in ppm. The value of 100% represents the reference concentration basis, while the subsequent values represent the remaining concentration profile after processing. Therefore, Table 2 should not be interpreted as a separate daily run in which each day’s initial concentration depends on the previous day’s final concentration.

The values in Table 2 are expressed as percentage concentration profiles, not raw ppm concentrations. The raw initial concentrations are shown in Table 1, while Table 2 presents the processed input data used for model development. For methylene blue, the value of 100% represents the reference concentration level, and the subsequent values indicate the remaining concentration percentage during the phytoremediation period. The same percentage basis was applied to Congo red to ensure consistency in the model input dataset. The removal efficiency and % methylene blue are calculated using Equations (1) and (2):

$$Methylene\ Blue\ Percentage = \frac{C_e}{C_0} \times 100\% \quad (1)$$

$$Removal\ Percentage = \frac{C_0 - C_e}{C_0} \times 100\% \quad (2)$$

where $C_0$ is the initial concentration (mg/L), $C_e$ is the final concentration (mg/L).

**Table 2.** Processed concentration variables used as Neural–Wiener model inputs

| Observation index | Methylene blue concentration ($x_1$) (%) | *Congo red* concentration ($x_2$) (%) | Control Variable | | |
|---|---|---|---|---|---|
| | | | Water Volume(ml) ($u_1$) | Glass Diameter (cm) ($u_2$) | Mass of *Lemna Minor* Plant (g) ($u_3$) |
| 1 | 100 | 100 | 200 | 9 | 2 |
| 2 | 8 | 100 | 200 | 9 | 2 |
| 3 | 6 | 79 | 200 | 9 | 2 |
| 4 | 7 | 79 | 200 | 9 | 2 |
| 5 | 4 | 81 | 200 | 9 | 2 |
| 6 | 5 | 81 | 200 | 9 | 2 |
| 7 | 7 | 69 | 200 | 9 | 2 |
| 8 | 5 | 69 | 200 | 9 | 2 |
| 9 | 6 | 77 | 200 | 9 | 2 |
| 10 | 7 | 77 | 200 | 9 | 2 |
| 11 | 6 | 64 | 200 | 9 | 2 |
| 12 | 5 | 64 | 200 | 9 | 2 |
| 13 | 6 | 82 | 200 | 9 | 2 |
| 14 | 3 | 82 | 200 | 9 | 2 |
| 15 | 0.25 | 59 | 200 | 9 | 2 |
| 16 | 0.29 | 59 | 200 | 9 | 2 |
| 17 | 0.25 | 77 | 200 | 9 | 2 |
| 18 | 0.24 | 77 | 200 | 9 | 2 |
| 19 | 0.15 | 70 | 200 | 9 | 2 |
| 20 | 0.22 | 70 | 200 | 9 | 2 |
| 21 | 0.25 | 76 | 200 | 9 | 2 |
| 22 | 0.18 | 76 | 200 | 9 | 2 |
| 23 | 0.16 | 75 | 200 | 9 | 2 |
| 24 | 0.19 | 75 | 200 | 9 | 2 |
| 25 | 0.18 | 75 | 200 | 9 | 2 |

The corresponding final treatment response is presented in Table 3 as dye removal percentage. Therefore, in this study, Table 2 represents the processed input concentration profiles, while Table 3 represents the corresponding output removal responses used for Neural–Wiener model training, validation, and testing.

Table 3 presents the corresponding output response used for model training and evaluation. The output variables were the removal responses of methylene blue and Congo red. The relationship between the input data in Table 2 and the output data in Table 3 was evaluated using correlation analysis. Since water volume, glass diameter and *Lemna minor* mass were kept constant at 200 mL, 9 cm and 2 g, respectively, these control variables did not contribute to output variation in the present dataset. The main varying inputs were therefore the processed methylene blue and Congo red concentration profiles over the observation period.

**Table 3.** Corresponding dye-removal responses used as Neural–Wiener model outputs

| Observation index | Methylene blue removal (%) | Congo red removal (%) |
|---|---|---|
| 1 | 92 | 0 |
| 2 | 94 | 21 |
| 3 | 93 | 21 |
| 4 | 96 | 19 |
| 5 | 95 | 19 |
| 6 | 93 | 31 |
| 7 | 95 | 31 |
| 8 | 94 | 23 |
| 9 | 93 | 23 |
| 10 | 94 | 36 |
| 11 | 95 | 36 |
| 12 | 94 | 18 |
| 13 | 97 | 18 |
| 14 | 100 | 41 |
| 15 | 100 | 41 |
| 16 | 100 | 23 |
| 17 | 100 | 23 |
| 18 | 100 | 30 |
| 19 | 100 | 30 |
| 20 | 100 | 24 |
| 21 | 100 | 24 |
| 22 | 100 | 25 |
| 23 | 100 | 25 |
| 24 | 100 | 25 |
| 25 | 100 | 25 |

The removal percentages in Table 3 represent the treatment response for each observation. The values reported in Table 3 therefore represent removal at this fixed measurement endpoint. The observation numbers 1–25 are experimental data indices and do not represent sequential treatment days. They were used as the output variables for model training, validation, and testing. The observations were arranged according to the experimental data index, and the next observation does not depend on the final concentration of the previous observation. The exact measurement endpoint for each removal response should be reported according to the experimental sampling record to avoid confusion between observation index and treatment duration.

The relationship between the input and output data was analysed based on the datasets presented in Tables 2 and 3. In Table 2, methylene blue concentration $(x_1)$and Congo red concentration $(x_2)$were used as the main input variables, while water volume $(u_1)$, glass diameter $(u_2)$, and mass of *Lemna minor* $(u_3)$were treated as control variables. Since the control variables were kept constant at 200 mL, 9 cm, and 2 g, respectively, their direct correlation with the output was not evaluated.

The output data in Table 3 show the response of the phytoremediation system in terms of methylene blue and Congo red concentrations after treatment. Based on the correlation analysis, methylene blue input concentration showed a negative correlation with the methylene blue output response. This indicates that as the methylene blue concentration in the system decreased, the treatment response increased. A decrease in the remaining dye concentration naturally corresponds to an increase in removal percentage, according to the conservation of

mass. A similar trend was also observed for Congo red, although the relationship was less consistent due to fluctuations in the experimental data.

The correlation analysis showed that the methylene blue input profile had an inverse relationship with the methylene blue removal response, indicating that lower remaining dye concentration corresponded to higher removal performance. Congo red showed a less consistent relationship because the removal response fluctuated across the experimental observations. This behaviour suggests that Congo red removal by *Lemna minor* may be more variable than methylene blue removal under the tested conditions. However, because the dataset contained only 25 observations, the correlation result should be interpreted as an exploratory analysis rather than a definitive statistical relationship.

### *2.3. Model Methods*

#### *2.3.1. Feedforward Neural Network*

The Feedforward Neural Network (FFNN) is a widely used neural network structure for classification and regression problems [19]. As illustrated in Figure 3, the FFNN consists of an input layer, one or more hidden layers, and an output layer. The training performance of the model depends on the selected network architecture, particularly the number of hidden layers and hidden neurons. The overall model used five process variables: methylene blue concentration, Congo red concentration, water volume, container diameter, and *Lemna minor* mass. In the Neural–Wiener structure, the two intermediate outputs generated by the state-space block were supplied to the FFNN nonlinear block. The FFNN consisted of one hidden layer, with the number of hidden nodes varied from 20 to 200 in increments of 20. The output layer contained two nodes representing the predicted removal percentages of methylene blue and Congo red. The best-performing configuration contained 140 hidden nodes.

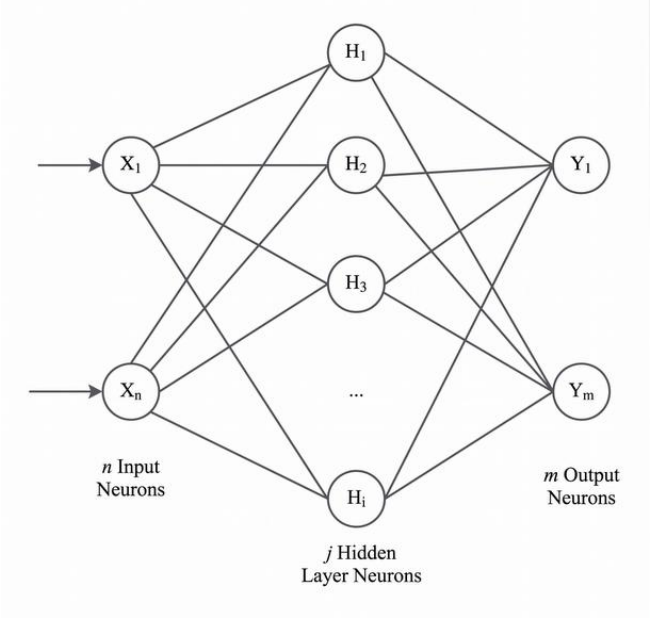



**Figure 3**. Feedforward Neural Network architecture.

*2.3.2. State-Space Model*

The state-space model is a mathematical representation used to describe dynamic systems [20]. It relates the system inputs, state variables, and outputs through state and output equations. The general continuous-time state-space model is expressed as:

$$\dot{x}(t) = A(t)x(t) + B(t)u(t) \tag{3}$$

$$y(t) = C(t)x(t) + D(t)u(t) \tag{4}$$

where $A(t)$ is the state matrix, $B(t)$ is the input matrix, $C(t)$ is the output matrix, and $D(t)$ is the direct transmission matrix. The linear state-space block used in this study is shown in Figure 4.

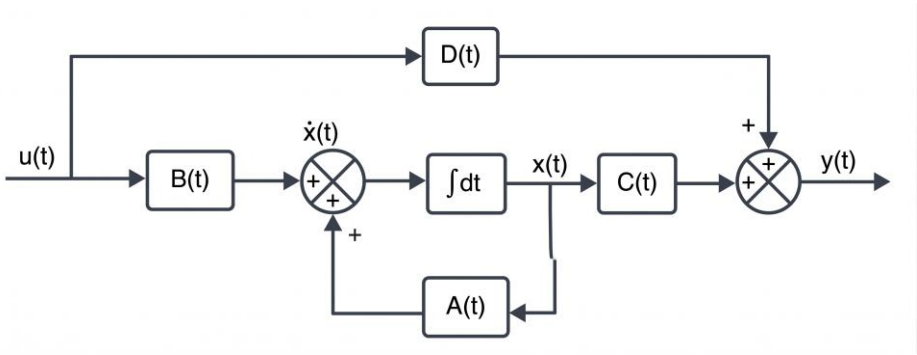



**Figure 4**. Linear block diagram in state-space form.

*2.3.3 Neural–Wiener Model*

The Neural–Wiener model combines a linear dynamic block with a nonlinear neural network block. In this study, the linear block was represented using a state-space model, while the nonlinear block was developed using an FFNN. The general structure of the Neural–Wiener model is shown in Figure 5.

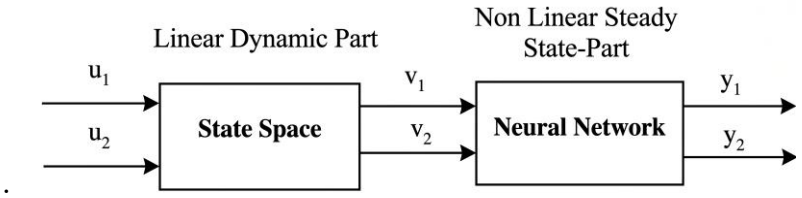



**Figure 5.** Neural–Wiener model structure.

In this study, the input vector $u(k)$represents the processed dye concentration inputs obtained from Table 2. These inputs include the methylene blue and Congo red concentration profiles, while water volume, glass diameter and *Lemna minor* mass were retained as controlled variables. The output vector $y(k)$represents the corresponding methylene blue and Congo red removal responses listed in Table 3. The state vector $x(k)$represents the internal dynamic states identified by the state-space model. These states are mathematical variables generated during system identification and do not correspond directly to a single measured physical parameter.

The input-output data were first identified using the MATLAB n4sid command to obtain the linear state-space model. The output from this block was then used as the intermediate variable for the nonlinear FFNN block. The discrete state-space equations are given as:

$$x(k+1) = Ax(k) + Bu(k) \tag{5}$$

$$v(k) = Cx(k) + Du(k) \tag{6}$$

where $x(k)$ is the state vector, $u(k)$ is the input vector, and $v(k)$ is the intermediate output from the linear block.

The nonlinear block was developed using the MATLAB newff command. The model was trained and evaluated using three data-partitioning ratios, namely 35% training, 30% validation and 35% testing; 40% training, 30% validation and 30% testing; and 50% training, 25% validation and 25% testing. The number of hidden nodes in the feedforward neural network was varied from 20 to 200 in increments of 20 to examine the effect of network complexity on prediction accuracy and computational time. The final model was selected based on the combined consideration of MSE, MAE, WMAPE and computation time.

The FFNN used the intermediate variable $v(k)$ as the input and produced the final model output $y(k)$. The neural network output can be written as:

$$y(k) = w_0 + \sum_{i=1}^{K} w_i^2 \ \varphi\left(w_{i,0}^1 + w_{i,1}^1 v(k)\right) \tag{7}$$

where $w_0$ is the bias, $w_{i,j}^1$ represents the first-layer weights, $w_i^2$ represents the second-layer weights, $\varphi$ is the nonlinear activation function, and $K$ is the number of hidden nodes. By combining the state-space and FFNN blocks, the output of the Neural–Wiener model can be expressed as:

$$y(k) = w_0 + \sum_{i=1}^{K} w_i^2 \ \varphi\left\{w_{i,0}^1 + w_{i,1}^1 [Cx(k) + Du(k) + e(k)]\right\} \tag{8}$$

where $e(k)$ represents the model error.

The Neural–Wiener model was therefore used as a data-driven dynamic model that maps the processed input concentration profile to the corresponding dye-removal response. Time, represented by the day or data index, was used to preserve the sequence of the experimental observations. No additional operating parameter was independently varied during the simulation beyond the concentration profiles and the indexed experimental sequence.

### *2.3.4. Error Analysis*

The prediction performance of the model was evaluated using Mean Squared Error (MSE), Mean Absolute Error (MAE), and Weighted Mean Absolute Percentage Error (WMAPE).

These error indices were used to measure the difference between the actual and predicted values [11]. MSE and MAE were calculated based on the percentage removal response and therefore follow the same percentage-response scale used in the output data. WMAPE was expressed as a relative error and may be reported as a fraction or converted into percentage form by multiplying by 100. These error metrics were used only to compare model configurations within the present dataset.

$$\text{MSE} = \frac{1}{n}\sum_{i=1}^{n}(\hat{y}_i - y_i)^2 \tag{9}$$

$$\text{MAE} = \frac{1}{n}\sum_{i=1}^{n}|\hat{y}_i - y_i| \tag{10}$$

$$\text{WMAPE} = \frac{\sum_{i=1}^{n}|Y_i - \hat{Y}_i|}{\sum_{i=1}^{n}|Y_i|} \times 100\% \tag{11}$$

where $y_i$ or $Y_i$ represents the actual value, $\hat{y}_i$ or $\hat{Y}_i$ represents the predicted value, and $n$ is the total number of data points. A flowchart of the overall model-development procedure has been added in Appendix 1 to illustrate the sequence of data preparation, model construction, training, and evaluation.

The error values were calculated based on the percentage removal response used as the model output. Therefore, MSE and MAE follow the percentage-response scale of the output data, while WMAPE is a relative error value. These metrics were used to compare model configurations within the present dataset and should not be interpreted as raw concentration errors in ppm.

## 3. Results and Discussion

### *3.1. Neural-Wiener (NW) Model*

The Neural–Wiener model developed in this study consists of two main blocks: a linear state-space block and a nonlinear neural network block. The state-space block was first used to identify the dynamic relationship between the input and output data. The output from this block was then used as the intermediate variable for the nonlinear neural network model.
The model was tested using the experimental input and output datasets for methylene blue and Congo red removal by *Lemna minor*. The identified state-space model is expressed as:

$$\begin{aligned} \boldsymbol{x}(k) &= \boldsymbol{A}\boldsymbol{x}(k) + \boldsymbol{B}\boldsymbol{u}(k) + \boldsymbol{K}\, e(k) \\ \boldsymbol{y}(k) &= \boldsymbol{C}\boldsymbol{x}(k) + \boldsymbol{D}\boldsymbol{u}(k) + e(k) \end{aligned} \tag{12}$$

where $x(k)$is the state vector, $u(k)$is the input vector, $y(k)$is the model output, and $e(k)$is the prediction error. The matrices $A$, $B$, $C$, $D$, and $K$represent the state, input, output, direct transmission, and error gain matrices, respectively.

In this study, the identified state-space model produced a 10-state system with matrix dimensions of $A_{10\times10}$, $B_{10\times6}$, $C_{6\times10}$, and $D_{6\times6}$. The full numerical values of the identified

matrices are shown in the Appendix 2. The identified state-space model contained 10 states, and the corresponding $A$, $B$, $C$, and $D$ matrices represented the state dynamics, process inputs, model outputs, and direct transmission, respectively. The direct transmission matrix, $D$, was obtained as a zero matrix, indicating that there was no direct feedthrough from the input to the output. The error gain matrix, $K$, was also obtained as a zero matrix, suggesting that the model output was mainly determined by the identified state-space dynamics.

The state-space model provided the linear dynamic response of the phytoremediation system. However, since the removal of methylene blue and Congo red by *Lemna minor* involves nonlinear behaviour, the neural network block was added to improve the prediction capability of the model. The combined Wiener Neural model was then used to simulate the concentration profiles of methylene blue and Congo red.

The simulation results presented in Figures 6 and 7 show that the Neural–Wiener model captured the general concentration profiles of Congo red and methylene blue, respectively, while the corresponding prediction errors and computation times are summarised in Table 4. This indicates that the combination of a state-space model and neural network structure is suitable for modelling the dynamic and nonlinear behaviour of dye removal using *Lemna minor*.

After testing, the tested model is used as the FFNN model design in the Nonlinear Neural–Wiener block to simulate the best concentration value for the simulated solution of phytoremediation in *Lemna minor*. To calculate the MSE error against the semi-empirical methylene blue and Congo red concentrations, the results of the Neural–Wiener output were used to create a comparison graph, as shown in Table 4.

Table 4 presents the accuracy performance of the Neural–Wiener (NW) model using different data-splitting ratios and numbers of hidden nodes. The model performance was evaluated using MSE, MAE, WMAPE, and computation time. The results show that the number of hidden nodes has a significant effect on model accuracy and computational time. However, increasing the number of hidden nodes does not always improve the model performance. For example, in the 35% training, 30% validation, and 35% testing split, the MSE fluctuated as the number of hidden nodes increased. The lowest error was obtained at 140 hidden nodes, with an MSE of 0.0005, MAE of 0.0001, and WMAPE of 0.00001. This result indicates that the NW model with 140 hidden nodes gave the best prediction performance for this data split. It also required the shortest computation time, which was 1.5210 s.

For the 40% training, 30% validation, and 30% testing split, the best performance was obtained at 20 hidden nodes, with an MSE of 0.5514, MAE of 0.1322, and WMAPE of 0.0232. Although the model with 160 hidden nodes gave the lowest MAE and WMAPE in this split, its computation time was very high, reaching 573.0647 s. This suggests that increasing the model complexity may increase the computational burden without giving a major improvement in prediction accuracy.

For the 50% training, 25% validation, and 25% testing split, the lowest MSE was obtained at 60 hidden nodes, with a value of 0.5603. However, the lowest MAE and WMAPE were

obtained at 160 hidden nodes. This shows that different accuracy indicators may suggest different optimal model structures. Therefore, model selection should consider both prediction accuracy and computation time.

The NW model showed good prediction ability for the phytoremediation system. The best overall performance was obtained using the 35% training, 30% validation, and 35% testing split with 140 hidden nodes. The dataset contained only 25 observations and showed repeated concentration patterns. Therefore, the very low MSE, MAE and WMAPE values may indicate close fitting to the available data or possible overfitting. Additional independent experimental data are required to confirm whether the selected Neural–Wiener structure can reliably predict new phytoremediation conditions.

**Table 4.** NW model accuracy value results

| Splitting Data | Hidden Node | MSE | MAE | WMAPE | Computation time (s) |
|---|---|---|---|---|---|
| 35% Data Training, 30% Data Validation dan 35% Data Testing | 20 | 0.6288 | 0.2620 | 0.0493 | 31.8775 |
| | 40 | 1.1333 | 0.1869 | 0.0345 | 15.8470 |
| | 60 | 2.2392 | 0.5930 | 0.1170 | 15.7827 |
| | 80 | 1.1970 | 0.1500 | 0.0307 | 24.3604 |
| | 100 | 0.3444 | 0.1056 | 0.0191 | 39.2028 |
| | 120 | 3.1187 | 0.4475 | 0.0970 | 25.0298 |
| | 140 | 0.0005 | 0.0001 | 0.00001 | 1.5210 |
| | 160 | 0.7640 | 0.1039 | 0.0216 | 149.6752 |
| | 180 | 4.5202 | 0.6153 | 0.1212 | 40.1893 |
| | 200 | 1.4147 | 0.3588 | 0.0727 | 40.9045 |
| 40% Data Training, 30% Data Validation dan 30% Data Testing | 20 | 0.5514 | 0.1322 | 0.0232 | 13.8761 |
| | 40 | 0.9225 | 0.3182 | 0.0597 | 13.7726 |
| | 60 | 0.8489 | 0.2725 | 0.0529 | 16.4439 |
| | 80 | 0.9023 | 0.2480 | 0.0501 | 18.5086 |
| | 100 | 1.0404 | 0.1414 | 0.0287 | 27.9932 |
| | 120 | 4.4353 | 0.3077 | 0.0655 | 61.2400 |
| | 140 | 0.8422 | 0.1686 | 0.0349 | 25.1759 |
| | 160 | 0.5719 | 0.0984 | 0.0206 | 573.0647 |
| | 180 | 1.6578 | 0.4764 | 0.1019 | 49.0582 |
| | 200 | 1.4916 | 0.4060 | 0.0833 | 72.76889 |
| 50% Data Training, 25% Data Validation dan 25% Data Testing | 20 | 0.9626 | 0.1617 | 0.0274 | 12.7968 |
| | 40 | 1.1390 | 0.1891 | 0.0362 | 26.9336 |
| | 60 | 0.5603 | 0.1704 | 0.0318 | 22.3696 |
| | 80 | 1.1604 | 0.1715 | 0.0348 | 25.7993 |
| | 100 | 0.8592 | 0.0943 | 0.0194 | 66.3430 |
| | 120 | 3.1904 | 0.6669 | 0.1334 | 31.4691 |
| | 140 | 0.7584 | 0.2140 | 0.0438 | 36.9557 |
| | 160 | 0.8041 | 0.0923 | 0.0192 | 68.6127 |
| | 180 | 0.8968 | 0.1117 | 0.0225 | 92.1616 |
| | 200 | 1.5811 | 0.3904 | 0.0796 | 51.3856 |

Figures 6 and 7 present the best simulation results obtained using the Neural–Wiener model for Congo red and methylene blue concentrations, respectively. The best model was achieved using a data division of 35% training, 30% validation, and 35% testing, with 140 hidden nodes.

Based on Table 4, this configuration produced the lowest error values, with an MSE of 0.0005, MAE of 0.0001, WMAPE of 0.00001, and computation time of 1.5210 s. These results indicate that the selected Wiener Neural model was able to provide highly accurate prediction performance with low computational time.

The very low error obtained for the 35% training, 30% validation and 35% testing split with 140 hidden nodes should be interpreted carefully. Since the dataset was small and contained repeated concentration patterns, the low error may partly reflect close fitting to the available dataset. Therefore, the result should not be considered proof of strong generalisation. Additional independent experimental data are required before the model can be confirmed as robust for broader phytoremediation prediction.

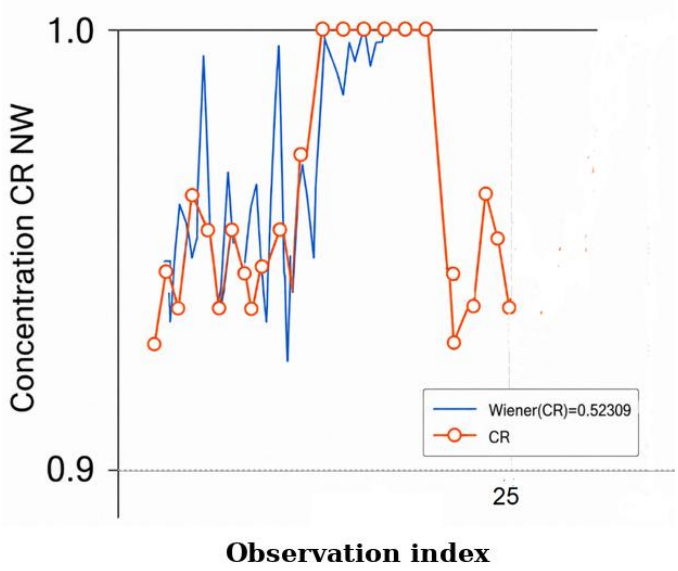



**Figure 6.** Neural–Wiener model simulation result for Congo red concentration profile. The x-axis represents the observation index, and the y-axis represents the processed Congo red concentration profile (%).

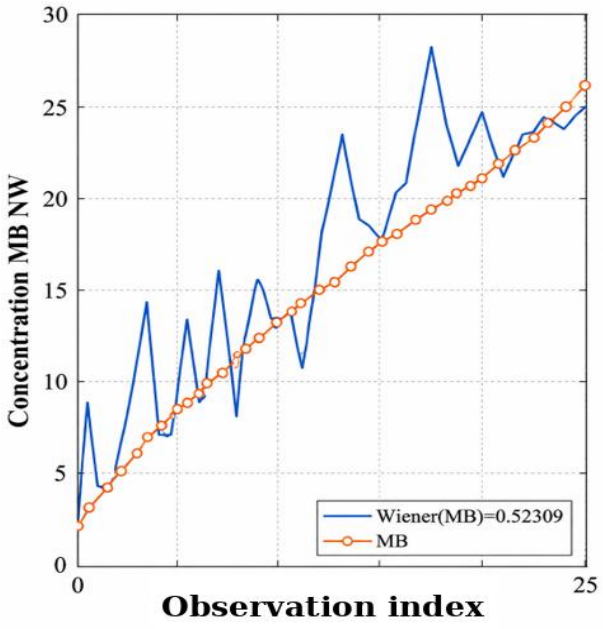



**Figure 7.** Neural–Wiener model simulation result for methylene blue concentration profile. The x-axis represents the observation index, and the y-axis represents the processed methylene blue concentration profile (%).

In Figure 6, the Congo red concentration shows a repeated pattern with values mostly between 0.92 and 1.00. The model was able to follow the general trend of the original Congo red data, particularly the repeated increase and decrease in concentration. This shows that the linear state-space block was able to capture the dynamic behaviour of the system, while the nonlinear neural network block improved the prediction of the concentration profile.

Figure 7 shows the simulation result for methylene blue concentration. The original data display a repeated increasing pattern followed by a sudden drop, which indicates a nonlinear and dynamic response during the phytoremediation process. The Neural–Wiener model was able to represent the increasing trend of methylene blue concentration, especially in the early data region. This suggests that the model can learn the relationship between the input variables and the output response of the phytoremediation system.

The results show that the Neural–Wiener model is suitable for modelling the phytoremediation process using *Lemna minor*. The combination of a state-space model and a feedforward neural network allows the model to describe both linear dynamic behaviour and nonlinear input-output relationships. The low values of MSE, MAE, and WMAPE confirm that the model has good prediction accuracy.

The plots in Figures 6 and 7 mainly show the ability of the Neural–Wiener model to reproduce the concentration-response pattern in the available dataset. They do not represent a full mechanistic simulation in which several process variables were independently varied. The model should therefore be regarded as a preliminary predictive tool for the tested experimental range, rather than a general phytoremediation model applicable to all dye concentrations, plant conditions or treatment durations.

## 4. Conclusions

This study applied a Neural–Wiener model to predict methylene blue and Congo red removal during *Lemna minor* phytoremediation. The model combined a linear state-space block with a nonlinear neural network block to represent the dynamic and nonlinear behaviour of the treatment process. The best performance was obtained using 35% training data, 30% validation data, and 35% testing data with 140 hidden nodes. This configuration produced the lowest error values, with an MSE of 0.0005, MAE of 0.0001, WMAPE of 0.00001, and computation time of 1.5210 s. The results show that the model could follow the general concentration-response patterns of methylene blue and Congo red in the available dataset. However, the findings should be interpreted as a preliminary modelling assessment because the dataset consisted of only 25 observations with repeated concentration patterns. Further validation using additional independent experiments with wider dye concentrations, treatment durations, and plant biomass conditions is recommended to confirm the robustness and generalisation ability of the model.

## Acknowledgments

The authors would like to thank the Mineral Technology Research Institute, the National Research and Innovation Agency (BRIN), and the ITERA mathematics study program for assisting with this research.

## Conflict of interest

The authors declare no conflict of interest.

## References

[1] A Kumar, A Kapoor, DB Pal. Removal of methylene blue and Congo red dyes using sustainable and eco-friendly bioadsorbents: A review. Asia-Pacific Journal of Chemical Engineering, 2025, 21(1), e70175, https://doi.org/10.1002/apj.70175

[2] SN Khan, L Anjum, A Arshad, S Ali, M Aleem, A Nasir. Nature-based solution for wastewater treatment and reuse using phytoremediation with floating plants. Water, 2025, 17(7), 1080, https://doi.org/10.3390/w17071080

[3] SK Bhagat, KE Pilario, BO Emmanuel, Tiyasha, M Yaqub, CE Onu, K Pyrgaki, MW Falah, AH Jawad, DA Yaseen, N Barka, ZM Yaseen. Comprehensive review on machine learning methodologies for modeling dye-removal processes in wastewater. Journal of Cleaner Production, 2023, 385, 135522, https://doi.org/10.1016/j.jclepro.2022.135522

[4] AS Sudibyo, FD Gunada, L Zakaria, FR Lumbanraja, FS Rohman, D Muhammad. Comparison of neural capabilities of Hammerstein, Neural-Wiener, and Hammerstein-Wiener models in modeling the limiting current of lanthanum electrodeposition. ASEAN Journal of Process Control, 2024, 2(2). Available online: https://mypcs.com.my/journal/index.php/ajpc/article/view/17 (Assessed on 26 May 2026)

[5] M Schoukens, K Tiels. Identification of block-oriented nonlinear systems starting from linear approximations: A survey. Automatica, 2017, 85, 272-292, https://doi.org/10.1016/j.automatica.2017.06.044

[6] P Frącz. Nonlinear modeling of the activated sludge process using the Hammerstein–Wiener structure. E3S Web of Conferences, 2016, 10, 00119, https://doi.org/10.1051/e3sconf/20161000119

[7] MS Gaya, MU Zango, LA Yusuf, M Mustapha, B Muhammad, A Sani, A Tijjani, N Wahab, M Khairi. Estimation of turbidity in a water treatment plant using Hammerstein–Wiener and neural network techniques. Indonesian Journal of Electrical Engineering and Computer Science, 2017, 5(3), 666-672, https://doi.org/10.11591/ijeecs.v5.i3.pp666-672

[8] SI Abba, V Nourani, G Elkiran. Multi-parametric modeling of a water treatment plant using an AI-based nonlinear ensemble. Journal of Water Supply: Research and Technology—Aqua, 2019, 68(7), 547-561, https://doi.org/10.2166/aqua.2019.078

[9] SMH Shah, SI Abba, MA Yassin, et al. New strategy based on Hammerstein–Wiener and supervised machine learning for identification of treated wastewater salinization in the Al-Hassa region, Saudi Arabia. Environmental Sciences Europe, 2024, 36, 114, https://doi.org/10.1186/s12302-024-00914-9

[10] H Han, J Qiao. Nonlinear model-predictive control for industrial processes: An application to a wastewater treatment process. IEEE Transactions on Industrial Electronics, 2014, 61(4), 1970–1982, https://doi.org/10.1109/TIE.2013.2266086

[11] M Ławryńczuk. Practical nonlinear predictive control algorithms for Neural–Wiener models. Journal of Process Control, 2013, 23(5), 696-714, https://doi.org/10.1016/j.jprocont.2013.02.004

[12] N Fitriana, S Kuntjoro. Kemampuan *Lemna minor* dalam menurunkan kadar linear alkyl benzene sulphonate. LenteraBio: Berkala Ilmiah Biologi, 2021, 9(2), 109-114, https://doi.org/10.26740/lenterabio.v9n2.p109-114

[13] R Irawanto. Fitoremediasi lingkungan dalam Taman Bali. Local Wisdom: Jurnal Ilmiah Kajian Kearifan Lokal, 2010, 2(4), 29-35.

[14] W. Lestari. Penggunaan Ipomoea aquatica Forsk. untuk fitoremediasi limbah rumah tangga. Prosiding Semirata, 2013, 1(1), 441–446.

[15] I Riwayati, N Fikriyyah, S Suwardiyono. Adsorpsi zat warna methylene blue menggunakan abu alang-alang (Imperata cylindrica) teraktivasi asam sulfat. Jurnal Inovasi Teknik Kimia, 2019, 4(2), 6-11, https://doi.org/10.31942/inteka.v4i2.3016

[16] Erwanto. Fotodegradasi zat warna methylene blue menggunakan TiO2/zeolit dengan penambahan ion nitrat (NO3). Undergraduate Thesis, Universitas Islam Negeri Maulana Malik Ibrahim, Malang, Indonesia, 2014, 1-103, http://etheses.uin-malang.ac.id/8264/1/09630050.pdf

[17] LW Hadayani, I Riwayati, RD Ratnani. Penurunan kadar zat warna methylene blue menggunakan eceng gondok (Eichhornia crassipes). Jurnal Momentum, 2015, 11(1), 19-23

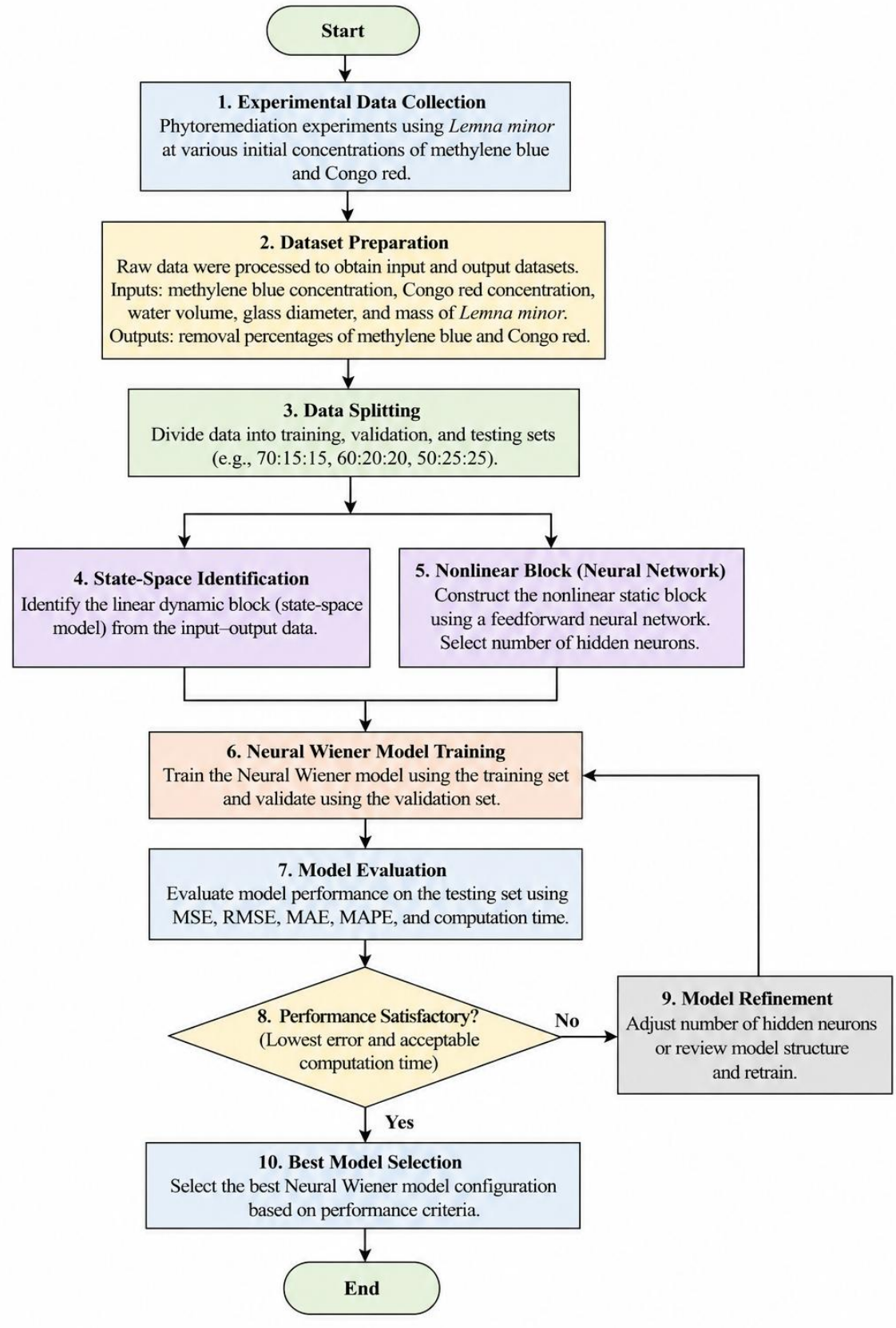
[18] EI Yakupova, LG Bobyleva, IM Vikhlyantsev, AG Bobylev. Congo red and amyloids: History and relationship. Bioscience Reports, 2019, 39(1), BSR20181415, https://doi.org/10.1042/BSR20181415

[19] NC Hammadi, H Ito. Improving the performance of feedforward neural networks by noise injection into hidden neurons. Journal of Intelligent and Robotic Systems, 1998, 21(2), 103-115, https://doi.org/10.1023/A:1007965819848

[20] J Schoukens, L Ljung. Nonlinear system identification: A user-oriented road map. IEEE Control Systems Magazine, 2019, 39(6), 28–99, https://doi.org/10.1109/MCS.2019.2938121

## Appendix 1

### Flowchart of Neural–Wiener Model Development



## Appendix 2

The following equations show the state-space results:

$$x(k) = Ax(k) + Bu(k) + K\,e(k)$$

$$y(k) = Cx(k) + Du(k) + e(k)$$

with

$$A_{10\times10} = \left[\bar{A}_{1(10\times10)} \quad \bar{A}_{2(10\times10)}\right]$$

where

$$\bar{A}_{1(10\times5)} = \begin{bmatrix} 1.4206 & -2.2404 & -2.0566 & -2.4041 & 1.2560 \\ 3.0818 & -2.9402 & -0.1602 & -1.2026 & 1.4494 \\ 3.6448 & -4.0466 & -0.4705 & -1.7122 & 2.1813 \\ -5.3108 & 7.0511 & 1.8816 & 3.9464 & -3.7616 \\ -3.4714 & 4.1915 & 0.5917 & 1.9822 & -1.5560 \\ 4.1004 & -4.6010 & -4.1955 & -3.4488 & 3.3257 \\ -3.2947 & 2.6549 & -0.2463 & 0.3316 & -1.3353 \\ 0.0642 & -0.0348 & -0.1372 & -0.2922 & 0.3175 \\ 1.8486 & -0.0190 & 4.9452 & 3.4690 & -0.4942 \\ 1.2206 & -1.8836 & -2.6744 & -2.4251 & 1.7074 \end{bmatrix}$$

$$\bar{A}_{2(10\times5)} = \begin{bmatrix} -0.0642 & -0.7401 & -0.7146 & 0.5623 & -0.7654 \\ 0.1362 & -0.6885 & 0.1159 & 0.5903 & -1.5735 \\ -0.5638 & -1.7637 & -0.3359 & 0.5867 & -0.4875 \\ 0.9700 & 3.4677 & 0.3537 & -0.7028 & 1.3248 \\ 0.1250 & 0.5889 & 0.7311 & -1.1883 & 0.9746 \\ -0.7727 & -3.3044 & 1.5581 & 0.2744 & -1.4336 \\ -0.2530 & 0.2881 & -1.4385 & -0.3040 & 1.9218 \\ 0.1511 & -0.2784 & 0.6937 & -0.4922 & -0.7417 \\ 0.7412 & 0.7658 & 2.7695 & -0.6685 & -1.8164 \\ -0.4255 & -1.8609 & -0.7893 & -0.0744 & -0.2403 \end{bmatrix}$$

$$B_{10\times6} = \left[\bar{B}_{1(10\times3)} \quad \bar{B}_{2(10\times3)}\right]$$

where

$$\bar{B}_{1(10\times3)} = \begin{bmatrix} 1.1792\times10^{+16} & 2.4029\times10^{+15} & -3.9428\times10^{+14} \\ 1.0422\times10^{+16} & 1.7719\times10^{+15} & -1.1552\times10^{+13} \\ 6.4748\times10^{+15} & 3.9692\times10^{+14} & 1.0982\times10^{+15} \\ -7.0008\times10^{+15} & -7.0443\times10^{+14} & -1.4354\times10^{+15} \\ -2.0340\times10^{+16} & -2.2535\times10^{+15} & -7.9929\times10^{+13} \\ 2.4195\times10^{+15} & 1.2322\times10^{+15} & 7.1353\times10^{+14} \\ -2.2845\times1^{+16} & -2.6138\times10^{+15} & 1.6819\times10^{+14} \\ 4.9615\times10^{+15} & 6.6273\times10^{+14} & -4.2539\times10^{+14} \\ -1.9756\times10^{+15} & -1.8526\times10^{+15} & -1.5580\times10^{+14} \\ 6.6961\times10^{+15} & 1.2830\times10^{+15} & -9.6989\times10^{+13} \end{bmatrix}$$

$$\bar{B}_{2(10\times3)} = \begin{bmatrix} -1.3885\times10^{+15} & -6.2483\times10^{+13} & -1.3885\times10^{+13} \\ -1.3185\times10^{+15} & -7.0008\times10^{+15} & -5.9331\times10^{+13} \\ -1.2124\times10^{+15} & -5.4558\times10^{+13} & -1.2124\times10^{+13} \\ 1.4220\times10^{+15} & 6.3988\times10^{+13} & 1.4220\times10^{+13} \\ 2.6089\times10^{+15} & 1.1740\times10^{+14} & 2.6089\times10^{+13} \\ -6.0530\times10^{+14} & -2.7238\times10^{+13} & -6.0530\times10^{+12} \\ 2.8062\times10^{+15} & 1.2628\times10^{+14} & 2.8062\times10^{+13} \\ -4.7205\times10^{+14} & -2.1242\times10^{+13} & -4.7205\times10^{+12} \\ 3.8941\times10^{+14} & 1.7523\times10^{+13} & 3.8941\times10^{+12} \\ -8.4750\times10^{+14} & -3.8138\times10^{+15} & -8.4750\times10^{+12} \end{bmatrix}$$

$$C_{6\times10} = \left[\bar{C}_{1(6\times2)} \quad \bar{C}_{2(6\times2)} \quad \bar{C}_{3(6\times2)} \quad \bar{C}_{4(6\times2)} \quad \bar{C}_{5(6\times2)}\right]$$

where

$$\bar{C}_{1(6\times2)} = \begin{bmatrix} -1.3735\times10^{-15} & 9.8187\times10^{-16} \\ -1.0308\times10^{-16} & 1.9402\times10^{-16} \\ 1.7475\times10^{-16} & -1.1542\times10^{-16} \\ -1.3735\times10^{-15} & 9.8187\times10^{-16} \\ -1.0308\times10^{-16} & 1.9402\times10^{-16} \\ 1.7475\times10^{-16} & -1.1542\times10^{-16} \end{bmatrix}$$

$$\bar{C}_{2(6\times2)} = \begin{bmatrix} -5.2776\times10^{-15} & -4.4286\times10^{-15} \\ 3.7325\times10^{-16} & 2.2136\times10^{-16} \\ -1.8303\times10^{-16} & -1.1594\times10^{-16} \\ -5.2776\times10^{-15} & -4.4286\times10^{-15} \\ 3.7325\times10^{-16} & 2.2136\times10^{-16} \\ -1.8303\times10^{-16} & -1.1594\times10^{-16} \end{bmatrix}$$

$$\bar{C}_{3(6\times2)} = \begin{bmatrix} 3.9828\times10^{-15} & -2.8686\times10^{-15} \\ 3.4359\times10^{-17} & 5.1162\times10^{-17} \\ 9.3539\times10^{-17} & -4.7858\times10^{-17} \\ 3.9828\times10^{-15} & -2.8686\times10^{-15} \\ 3.4359\times10^{-17} & 5.1162\times10^{-17} \\ 9.3539\times10^{-17} & -4.7858\times10^{-17} \end{bmatrix}$$

$$\bar{C}_{4(6\times2)} = \begin{bmatrix} -4.7918\times10^{-15} & -6.5932\times10^{-15} \\ 2.9417\times10^{-17} & 3.1216\times10^{-16} \\ -1.1534\times10^{-16} & -1.9160\times10^{-16} \\ -4.7918\times10^{-15} & -6.5932\times10^{-15} \\ 2.9417\times10^{-17} & 3.1216\times10^{-16} \\ -1.1534\times10^{-16} & -1.9160\times10^{-16} \end{bmatrix}$$

$$\bar{C}_{5(6\times2)} = \begin{bmatrix} -4.6069\times10^{-16} & 2.7943\times10^{-15} \\ -9.3836\times10^{-17} & -3.2001\times10^{-16} \\ 4.1893\times10^{-17} & 9.2386\times10^{-17} \\ -4.6069\times10^{-15} & 2.7943\times10^{-15} \\ -9.3836\times10^{-17} & -3.2001\times10^{-16} \\ 4.1893\times10^{-16} & 9.2386\times10^{-17} \end{bmatrix}$$

$$D_{6\times6}$$

where

$$D_{6\times6} = \begin{bmatrix} 0 & 0 & 0 & 0 & 0 & 0 \\ 0 & 0 & 0 & 0 & 0 & 0 \\ 0 & 0 & 0 & 0 & 0 & 0 \\ 0 & 0 & 0 & 0 & 0 & 0 \\ 0 & 0 & 0 & 0 & 0 & 0 \\ 0 & 0 & 0 & 0 & 0 & 0 \end{bmatrix}$$

$$K_{9\times6}$$

where

$$K_{9\times6} = \begin{bmatrix} 0 & 0 & 0 & 0 & 0 & 0 \\ 0 & 0 & 0 & 0 & 0 & 0 \\ 0 & 0 & 0 & 0 & 0 & 0 \\ 0 & 0 & 0 & 0 & 0 & 0 \\ 0 & 0 & 0 & 0 & 0 & 0 \\ 0 & 0 & 0 & 0 & 0 & 0 \\ 0 & 0 & 0 & 0 & 0 & 0 \\ 0 & 0 & 0 & 0 & 0 & 0 \\ 0 & 0 & 0 & 0 & 0 & 0 \end{bmatrix}$$